A NOVEL METHOD OF ANATOMICAL LANDMARK SELECTION FOR RIB CAGE 3D RECONSTRUCTION FROM BIPLANAR RADIOGRAPHY

Claudio Vergari[1*], Benjamin Aubert[1], Pauline Lallemant-Dudek[2], Thomas-Xavier Haen[1,3], Wafa Skalli[1]

Abstract

Methods to reconstruct anatomical structures in 3D are gaining interest in medicine because they give access to quantitative information on the patient's geometry. However, these methods are user-dependent and require a trained operator, which is time consuming and a source of error and unreliability.

The aim of this work was to validate a novel method of landmark selection to perform the 3D reconstruction of the rib cage from biplanar calibrated radiographies. The method uses digital painting for digitization of anatomical landmarks (eight ribs midlines, posterior extrema, sternum) to build a first estimate of the 3D ribcage geometry. Twenty scoliotic patients were included (Cobb angle: 43° ± 11°) and their ribcage was reconstructed twice with the proposed method by four trained operators.

Measurement reproducibility was similar to previously validated methods. Uncertainty (95% CI) was 2.3° for the rib hump measurement, 9.7 mm and 3.8 mm for maximal antero-posterior and lateral diameter, 395 cm^3 for ribcage volume. The method was qualitatively considered more user-friendly than previous versions, although it still requires a trained operator, and it took approximately 2 minutes of manual digitization.

The new method should facilitate diffusion of 3D quantitative analysis of ribcage in clinical routine.

Keywords: scoliosis; clinical parameters; 3D analysis; reliability; trunk; deformity

[1] *Arts et Metiers ParisTech, LBM/Institut de Biomecanique Humaine Georges Charpak, 151 bd de l'Hopital, 75013 Paris, France.*

[2] *Physical Medicine and Pediatric Rehabilitation, Armand Trousseau Hospital, Paris*

[3] *Ramsay Générale de Santé, Clinique Jouvenet, Paris, France*

** Corresponding author : Claudio Vergari, c.vergari@gmail.com*

Introduction

Scoliosis is a three-dimensional deformity of the spine and rib-cage which can lead to respiratory or locomotor impairment and to a decreased quality of life, when left untreated in its progressive form (Tones, Moss, & Polly, 2006; Weinstein, Dolan, Cheng, Danielsson, & Morcuende, 2008). Assessing the trunk of a scoliotic patient requires a 3D analysis of bones geometry, which can be useful for early treatment in brace design and evaluation (Nikita Cobetto et al., 2014; Thulbourne & Gillespie, 1976; Vergari et al., 2015), in the planning and evaluation of surgery (Jean Dubousset, Ilharreborde, & Le Huec, 2014; Gréalou, Aubin, & Labelle, 2002) and also for estimating pulmonary function in those cases where pulmonary function tests are not feasible (Yaszay, Bastrom, Bartley, Parent, & Newton, 2017).

Efforts have been made to quantify the 3D deformity of the rib cage from medical imaging, for instance with optical methods (Charles, Marcoul, Schaeffer, Canavese, & Diméglio, 2017; Hocquelet et al., 2016), computerized tomography (CT, Aaro & Dahlborn, 1981; Nankali, Torshabi, & Miandoab, 2017) and biplanar radiography (Cheriet, Laporte, Kadoury, Labelle, & Dansereau, 2007; Grenier, Parent, & Cheriet, 2013; Jolivet, Sandoz, Laporte, Mitton, & Skalli, 2010). Radiography has an advantage over CT and optical methods, as it is already performed in the clinical routine of adolescent idiopathic scoliosis (AIS) patients. Moreover, biplanar radiography systems, such as the EOS device, deliver a lower radiation dose to the patient than conventional radiography (Dietrich, Pfirrmann, Schwab, Pankalla, & Buck, 2013)

Reconstruction methods are often performed in two steps: an initial identification of anatomical landmarks, and a phase of fine adjustments. A semi-automatic method for rib cage 3D reconstruction from biplanar radiography was recently proposed (Aubert, Vergari, Ilharreborde, Courvoisier, & Skalli, 2016). Its initial phase required the identification of several anatomical landmarks to compute a first estimate of the rib cage 3D model: the user was asked to identify the most dorsal point of the 5^{th}, 8^{th} and 10^{th} ribs in the lateral view, the tips of 2^{nd}, 5^{th}, 8^{th} and 10^{th} ribs in the frontal view, and the most lateral points of the 2^{nd}, 5^{th}, 8^{th} and 10^{th} ribs in the frontal view. Moreover, the tips of 10^{th} left and right ribs were demanded in the lateral view as well, as stereo-corresponding points. Thus, 24 anatomical landmarks are required in total to compute a first estimate of the rib cage 3D model.

The identification of a point in x-ray image is an operator-dependent task, and it induces a high cognitive cost due to image interpretation, identification guidelines and counting ribs or vertebrae in images. This could result in large variability of the identification (Fig 1). In the previous work, although instructions were given to the operators to identify the rib midlines, the user would sometimes choose the rib's internal or external border (Fig 1, Aubert et al., 2016). Also, the user was asked to identify specific ribs but counting them was not always straightforward.

To overcome these difficulties, a novel simplified identification phase was developed in this work for fast and easier identification of the anatomical landmarks, which were necessary for the initialization of the 3D rib cage reconstruction. The aim was to develop

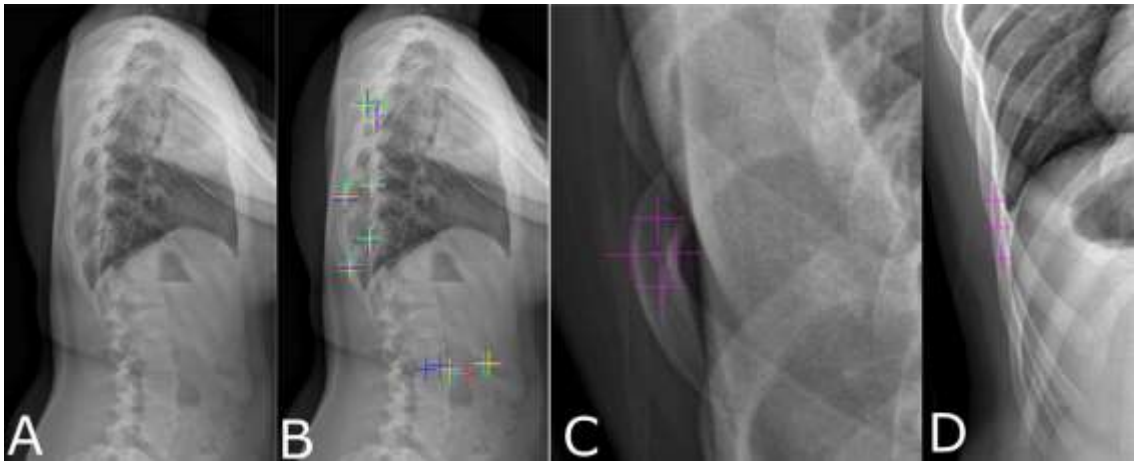

Fig. 1: (A) Original lateral x-ray and (B) source of reproducibility issues for points identification of anatomical landmark for different users (one colour each). (C) Examples of possibilities for the identification of most posterior point or (C) most lateral points.

an identification step that would provide an initial solution reliable enough to calculate main rib cage clinical parameters in mild to severe scoliosis.

Material and methods

Patients

Twenty adolescent idiopathic scoliotic patients (mean Cobb angle: 43° ± 11°, range: 18°-56°, mean age: 15 ± 2 years old, range 13-17) were retrospectively included in the study from a larger database. They underwent biplanar calibrated radiography in their routine follow-up with an EOS system (J Dubousset et al., 2005) (EOS Imaging, Paris, France). This system performs simultaneous frontal and lateral low-dose x-ray scan, yielding biplanar views of a calibrated 3D space. Data collection was approved by the ethical committee C.P.P. Ile-de-France VI (#6001).

Workflow

In brief, a 3D reconstruction of the spine and a simplified 3D reconstruction of the pelvis were performed using previously validated methods (Humbert, De Guise, Aubert, Godbout, & Skalli, 2009). These reconstructions were used to estimate the position of the rib joints at each level, and the position of the patient in the EOS calibrated 3D space. They were not included in the reproducibility study as their reliability has been thoroughly assessed (Ferrero et al., 2017; Ghostine et al., 2017; Glaser, Doan, & Newton, 2012; Ilharreborde et al., 2011; Rousseau, Brusson, & Lazennec, 2014). Then, the user had to paint the 2^{nd}, 5^{th}, 8^{th} and 10^{th} left and right ribs in the frontal view, the most posterior points of the ribs in the lateral view, and the position of the sternum in both views. Details are provided below.

Landmark identification method

Custom software allowed the user to select sets of pixels in x-ray images through digital painting (Figure 2). The identification in frontal view consisted of painting the 2^{nd}, 5^{th}, 8^{th} and 10^{th} left and right ribs. Each rib was painted independently in a step-by-step process, where the software automatically zoomed in on the x-ray at each of these rib levels, so the user did not have to count the ribs.

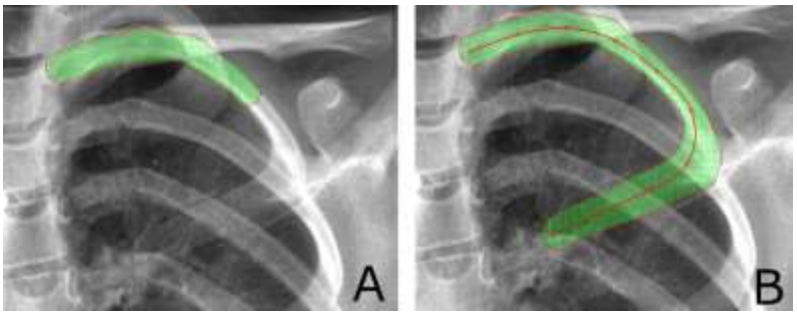

Fig. 2: Rib painting process (A) and (B) refinement of a spline fitting the painted pixel set.

The software estimated the position of the rib insertion automatically, as a result of the spinal 3D reconstruction previously done.

Each set of pixels 2D coordinates was first used to automatically estimate the position of the rib vertebral joint, the rib's distal tip and its most lateral point. A spline passing through these control points was then defined. By calculating the subset of pixels belonging to a circular neighbouring of additional control points (Figure 2B), the spline midline was fitted to the painted shape, giving the 2D rib trajectory. An example of rib painting is presented in Figure 3. Each set of pixels (i.e., each rib) was coloured with a semi-transparent colour to show the underlying radiography.

The identification in lateral view consisted of painting rounded spots (circular sets of pixels) on all visible posterior corners of the ribs; two separate sets were painted for left and right ribs. By assigning a label to a group of connected pixels, the centroid of each spot was computed. Then, cubic splines were fitted to the left and right sets of centroids to define the dorsal extremities of the rib cage (Fig. 4). The posterior portions of the ribs midline were constrained to this cubic spline.

Finally, the user placed a deformable 3D model of the sternum to fit its radiographic contours in the frontal and lateral x-rays (Figures 4 and 5). In total, the user had to paint 8 ribs (4 per side) in the frontal view and as many posterior rib corners as visible in the lateral view, in addition to the sternum template.

First estimate of 3D rib cage model

The principle of the first estimate of the 3D rib cage model was previously described (Aubert et al., 2016). Briefly, each rib was approximated by a parametric model consisting of two arcs, with continuous curvature at the junction

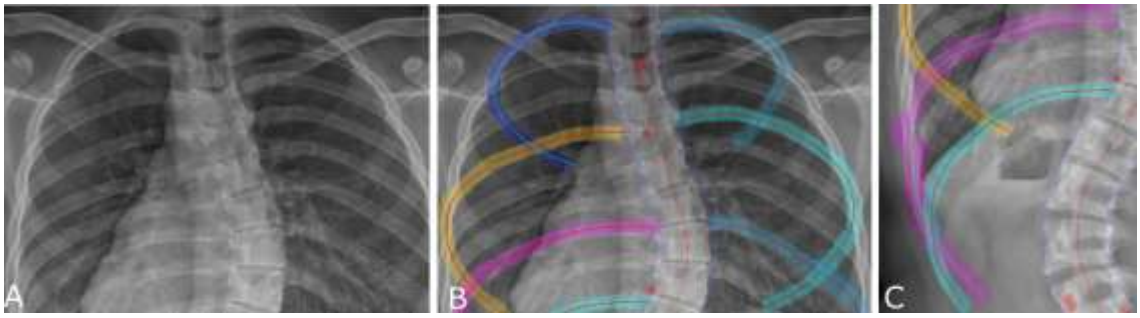

Fig. 3: Original frontal x-ray (A) and ribs painting examples (B). The template representing the sternum and the spinal midline are also visible. (C) Robust trajectory was extracted from pixel set even in presence of local imprecisions.

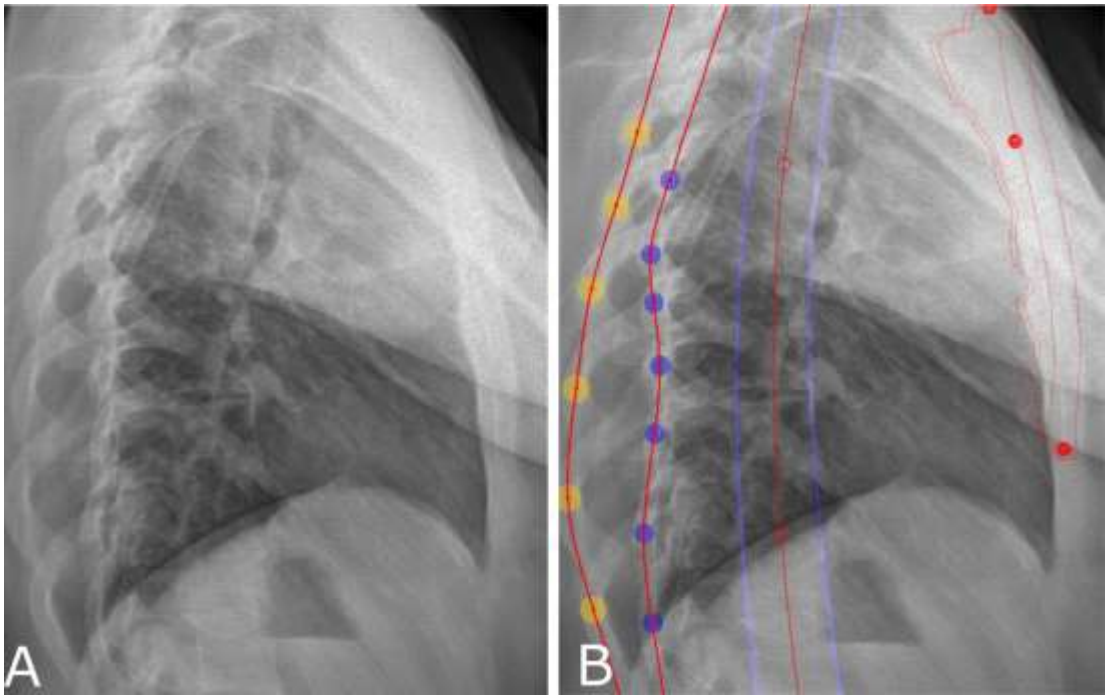

Fig. 4: (A) original lateral x-rayand (B) ribs posterior extremities identified by two sets of round spots. The centroids of each set of spots were connected by cubic splines, representing the dorsal left and right extremities of the rib cage. The template representing the sternum and the spinal midline are also visible

between them. Control ribs (2^{nd}, 5^{th}, 8^{th} and 10^{th}) passed through the previously detected control points (vertebral joint, rib tip, lateral point, most posterior point, Fig. 5), and they were used to define a bi-cubic surface approximating the rib cage. The remaining ribs were constrained to this surface and their trajectories were statistically inferred from the control ribs.

Side disambiguation in sagittal view

In the lateral view, it is not always straightforward to recognize the left or right ribs (Seoud, Cheriet, Labelle, & Dansereau, 2011). Side inversion can result in bias for the rib hump angle and incorrect rib geometry. In order to avoid this inversion, a decision model was developed, based on the hypothesis that the deformation of the dorsal rib cage should be consistent with the vertebral axial rotation (Fig. 6), e.g. a clockwise rotation of a vertebra should correspond to the patient's right-side ribs being more posterior in the lateral view. Rib hump was calculated for each level in a local vertebral frame (Fig. 6); then, the right and left user-defined spots were inverted and a virtual initial solution was generated to calculate "inverted rib humps". The sum of the rib hump differences between the actual and virtual inverted solution was calculated; a total value lower than 10° was considered not discriminant because it showed that the posterior corners were almost superimposed in lateral view, and the algorithm quit without further action. If the value was higher than 10° and the virtual inverted solution had smaller rib humps relative to the vertebra than the current solution (Fig. 6), an alert was shown to the user. Reliability of this

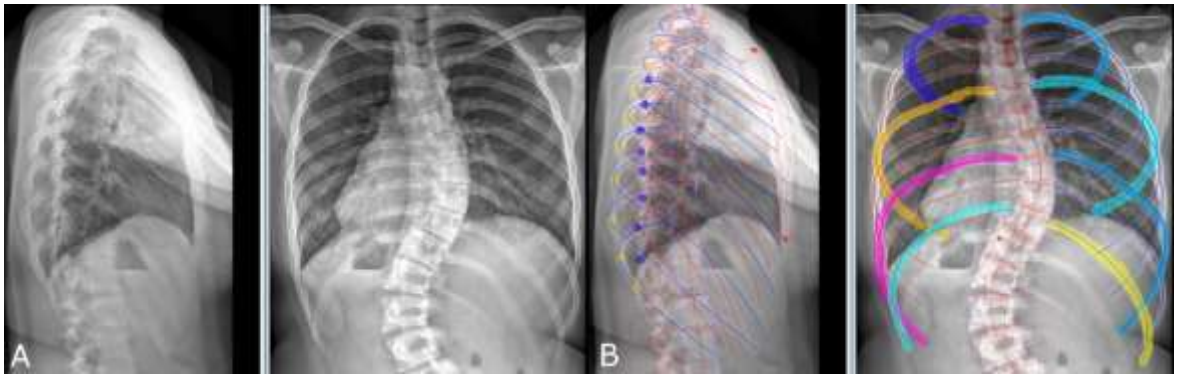

Fig. 5: (A) Original lateral and frontal x-rays and (B) rib cage 3D model fitted on painted identification

disambiguation algorithm was assessed as follows: the correct ribs side in lateral views was decided for the 20 included patients by consensus of three experienced operators. Then, the algorithm was run on a set of reconstructions based on this consensus, and on a virtual set where the sides were switched. Results were quantified in terms of true and false positives and negatives.

Reliability assessment

The initialization of the rib cage 3D reconstruction was performed twice by four experienced users on the 20 included patients (2x4x20 = 160 reconstructions). Two users were clinicians (authors P.L.-D. and T.-X.H.) and two were engineers (authors C.V. and B.A.). They all trained on a different dataset than the cohort included in this study. Intra-operator repeatability and inter-operator reproducibility of clinical and morphological parameters were calculated, in terms of twice the standard deviation, according to the international standard ISO 5725. Root mean squared differences (RMSD) were calculated between operators at each point of the 3D models, in order to obtain a map of differences.

Bland-Altman plots were used to compare the average clinical parameters for each patient of the current and the previous method (Aubert et al., 2016), which was performed on the same cohort. Data analysis was performed in Matlab 2014b (The MathWorks, Inc., Natick, MA, USA)

This first estimation is usually followed by a fine adjustment procedure to deform each rib in order to fit their midline projections to the frontal and lateral radiographies; this process, however, is identical to the previously described work (Aubert et al., 2016; Pietton, Bouloussa, Vergari, Skalli, & Vialle, 2017). Only the reliability of the first estimate is relevant for the current work. Reconstruction time was assessed for each 3D reconstruction with a stopwatch, by measuring the time between the first manual identification on the x-rays and the generation of the rib cage model. Computation time to generate the model was negligible (a few seconds).

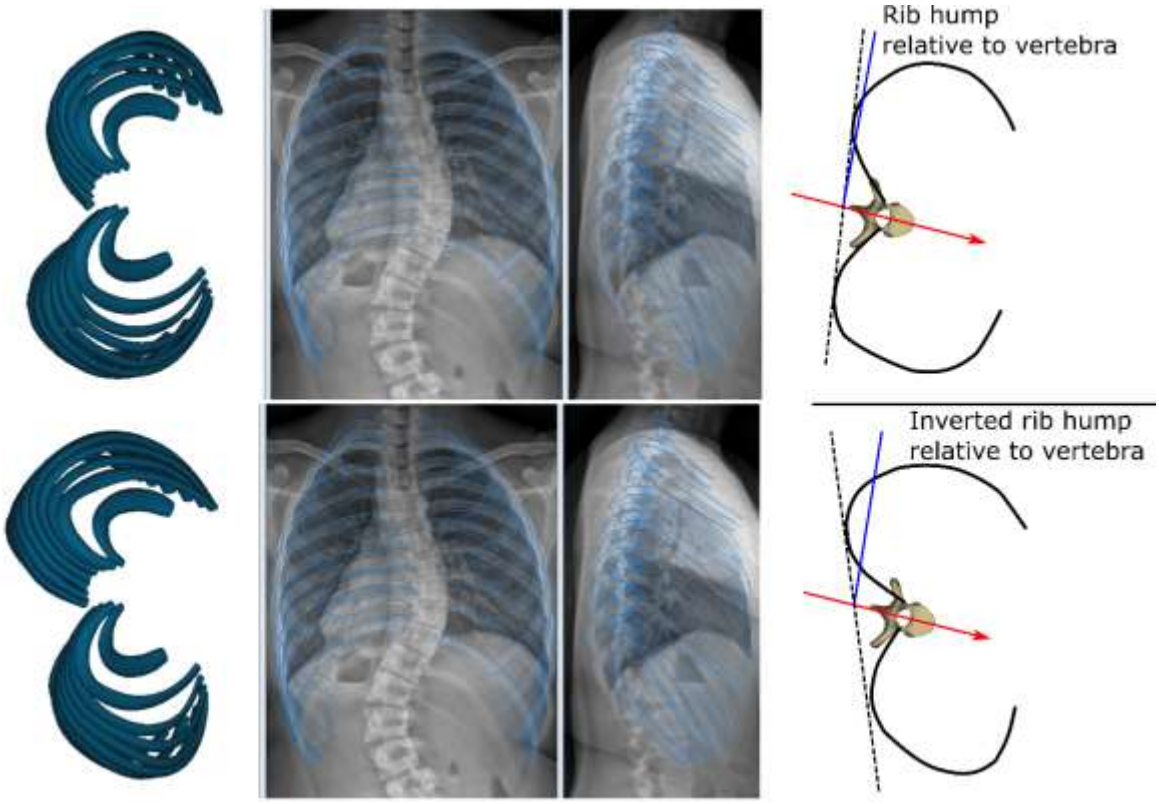

Fig. 6: Principle for decision model of potential left and right side inversion in the lateral view. The top row is the correct 3D reconstruction while in the bottom row the left and right ribs were inverted. Relative to the vertebra, the rib hump of the correct reconstruction is smaller than the inverted one.

Results

Table 1 shows the reliability of the proposed initialization method and a comparison with the previous method (Aubert et al., 2016), for which both the initialization and the fine adjustment results are reported. Reliability of almost all parameters was slightly improved by the current method relative to the previous initialization. Even when compared to the previous fine adjustment phase, some parameters (morphological parameters and the rib hump) were improved in the current method. Interestingly, uncertainty of volume estimation was larger in the current method (395 cm^3 in the current work against 306 cm^3 in the previous one); however, given the average volume of 4395 cm^3 in the current cohort (Table 1), this corresponds to only a 2% increase in uncertainty ((395 – 306)/4395*100 % = 2 %).

Figure 7 shows the comparison of the current method with the previously validated one, through Bland-Altman plots of the clinical parameters. Most of the differences are within the previous method's measurement uncertainty, confirming that the two methods are equivalent.

RMSD maps (Fig. 8, 3D model) show that the highest differences between users were concentrated at the tip of the sternum, were RMSDs were between 10 mm and 23 mm. Among the ribs,

Table 1: Reproducibility of intra and inter-observer results with 95% CI expressed in parameter units for the previous and the proposed method at the first estimate step.

	Aubert et al (2016)			Current work	
	Reproducibility of first estimate	Reproducibility of fine adjustment	Parameter mean (SD)	Reproducibility of first estimate	Parameter mean (SD)
Morphological parameters					
Length(mm)	17.5	15	233 (53)	11.8	234 (51)
Maximum width (mm)	5.5	5.3	67.5 (15.5)	4.2	67 (15)
Chord length (mm)	9.4	9.4	151 (39)	7.7	149 (38)
Area (mm^2)	34^2	30.4^2	63^2 (42^2)	26.5^2	62^2 (39^2)
Ribs orientation					
Frontal (°)	8	5.2	26 (12)	5.2	25 (12)
Sagittal (°)	6	5.5	40 (9)	5.9	42 (9.4)
Rib cage parameters					
Volume (cm3)	306	294	4528 (825)	395	4395 (807)
Max Rib Hump (°)	3.6	5	4 (6)	2.3	4 (6.7)
Max antero-posterior diameter (mm)	10	9.3	131 (12)	9.7	128 (11)
Max lateral diameter (mm)	4.3	3.2	223 (17)	3.8	224 (17.6)
Spinal penetration index (%)	1.3	1.2	5 (1)	1.4	5.8 (1)

differences were lower than 10 mm, and lower than 5 mm in the dorsal region.

The disambiguation algorithm had 0 false positives, i.e. it never suggested inverting ribs sides when the reconstruction was correct. However, it suffered from 10 false negatives (50 %) when it did not detect the inversion. This corresponds to a specificity of 100 % and a sensitivity of 67%.

The mean identification time on both views was 2 minutes, ranging between 1 and 4 minutes.

Discussion

A novel method to identify relevant landmarks for the 3D reconstruction of the rib cage in biplanar radiographies was presented and validated in the present work. Landmark selection is a common step of several quantitative methods of medical imaging analysis, from the measurement of the 2D Cobb angle in a frontal x-ray to the segmentation of CT scans. The method of selection and the instructions provided to the operator can have an impact on the reconstruction time and on the reliability of the results. The previous method we presented had instruction such as “pick the most lateral point of the n^{th} rib in lateral view”. This is

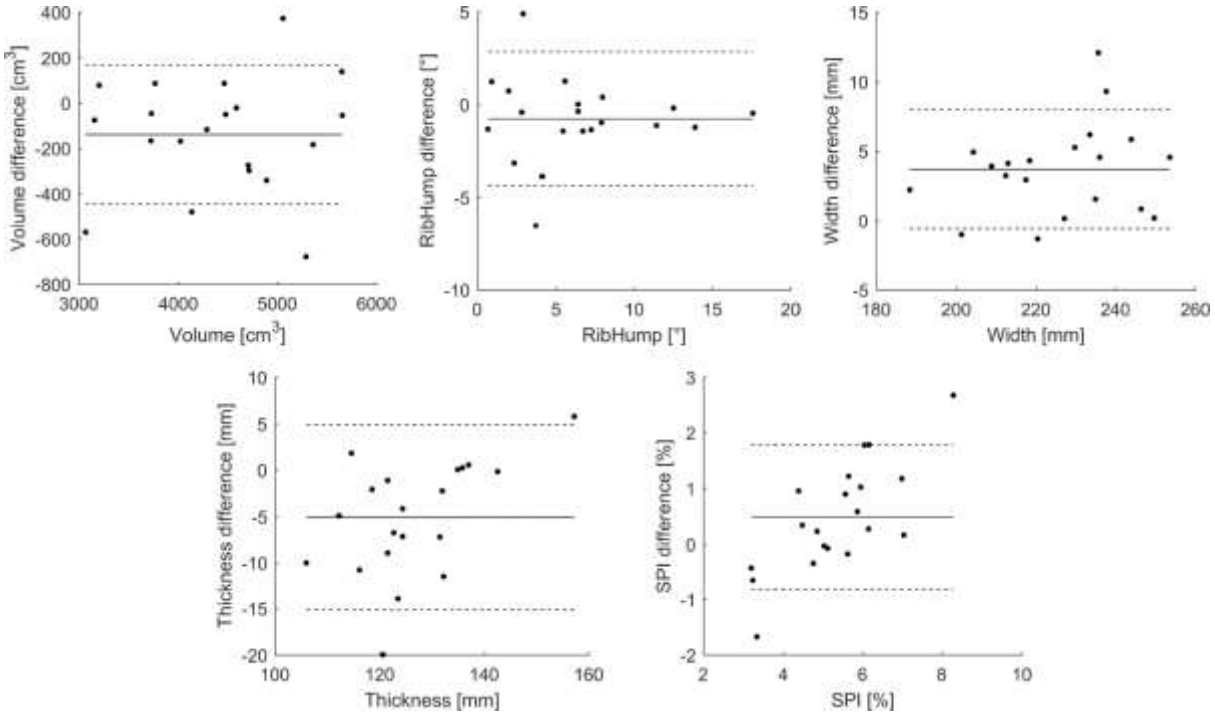

Figure 7. Bland-Altman plots comparing the current method with the previously validated one. Differences are based on the mean differences between methods for each patient. The horizontal dashed lines represent the measurement uncertainty of the previous method; most of the differences are within this uncertainty, confirming that the two methods are equivalent

imprecise since different operators will select the inner or outer rib border, or its midline (Figure 3C). Moreover, it could be time consuming and prone to errors, especially for beginners, because operators had to count the rib levels.

The main innovative feature of the present work is that users were asked to paint anatomical structures, rather than accurately select them through single points. The painting of the eight key ribs from costo-vertebral joint to the bony tip provided a robust rib trajectory and length in posteroanterior view. In lateral view, colored spots were used to identify the posterior rib's endings of as many visible ribs as possible. In the high thoracic region, posterior corners are not easily identified as they can be hidden by the arms. In the lower thoracic region, they can look less like corners and more like smooth curves, and thus be harder to identify. Therefore, the directive for the lateral view was intentionally unprecise: the user could identify only those points he/she felt confident of, and the remaining parts were statistically inferred (Fig. 4).

This method yielded a smooth trajectory for a given rib, and it was not too sensitive to coarse painting (Fig. 3B). The user instructions and training were simplified with this user-friendly rib painting, since coarsely painting ribs does not require specialized training or in-depth anatomical knowledge. The implemented software also automatically zoomed in the needed rib levels, eliminating the need of counting the ribs. This was possible using the available personalized 3D reconstruction of the spine. The

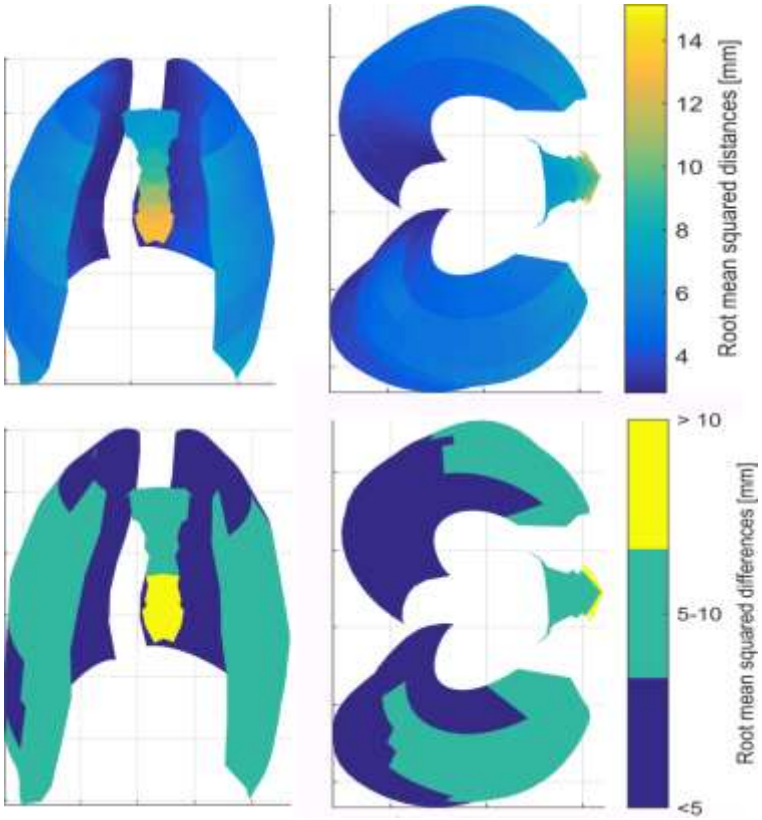

Figure 8. Root mean squared differences of 3D reconstructions between operators. The second row shows binned values. Differences are lower than 10 mm for the rib cage, and highest errors are concentrated on the distal tip of the sternum.

reconstructions were performed on a standard desktop PC with a mouse, but the method is potentially ready for tablets with touchscreens.

The side disambiguation detection had a perfect specificity of 100%, which is the true positive rate. In other words, there were no false positives, and the algorithm never offered to switch left and right side when the operator correctly chose them. This is very important, as the algorithm should not be allowed to worsen a good reconstruction. The drawback is that it had poor sensitivity, since it was only able to detect 50 % of the forced side inversions. However, 7 out of the 20 tested patients had a very symmetrical ribcage, with a rib hump lower than 5°, and the algorithm decided not to intervene. Such sensitivity means that the operator must be trained to recognize the left and right ribs in the lateral radiography. Indeed, the disambiguation algorithm is intended as a failsafe: it was never activated in the 160 reconstructions performed by trained users.

Rib cage sides can be recognized by observing the axial rotation of the vertebrae at the same level of the rib, as the algorithm tries to do (e.g., a clockwise rotation of the vertebra will be accompanied by a clockwise rotation of the ribcage, so the patient's right side will be more posterior as shown in Fig. 6). Moreover, the operator can observe the apparent size of the ribs on the lateral radiography: the ribs closer to the x-ray source will appear larger because of depth-dependent magnification artefact (Macovski, 1983). The side disambiguation detection could be improved using image analysis. A relevant approach was developed by Serrurier et al for femoral condyle disambiguation (Serrurier, Quijano, Nizard, & Skalli, 2012); the method was based on digital radiograph reconstructed from 3D reconstruction and a decision algorithm exploiting image similarity.

While the method was validated on images which were acquired on an EOS system, it can potentially be applied to

any couple of biplanar calibrated radiographies, such as digitally generated ones from CT-scans (Aubert et al., 2016; Dworzak et al., 2010; Sabourin et al., 2010) or those obtained with conventional radiography and rotary platforms (Grenier et al., 2013; Mitton et al., 2008).

Previous work from Dworzak et al (2010) aimed at reconstructing rib surfaces, which convey more information than rib midlines. However, their algorithm was preliminary tested on binary digitally generated biplanar radiographies of rib cages, i.e., the radiographies did not contain soft tissues. Moreover, no in-depth information was given about the initial manual labeling of the ribs. The present work was validated on in-vivo patient's biplanar calibrated radiographies.

The method proposed by Grenier et al. (2013) requires inputting 4 points per rib and image analysis amounting to an average of 40 minutes per reconstruction; for comparison, the proposed method requires a 2-minutes initialization.

Largest differences between users were concentrated on the sternum, and in particular on its distal tip. This is because the sternum has limited visibility in frontal view, and while the position of its proximal ending can be inferred from the clavicles, identification of the distal tip remains subjective. Also in the lateral view, the sternum can often be hidden by the arms. This introduces a degree of uncertainty on the overall shape of the ribcage, and in particular on its volume and thickness. A fine adjustments step for the ribs can still be performed also after the proposed initialization, and it was recently validated for severe scoliosis (Table 1, (Pietton et al., 2017)). While this fine adjustment would not have much impact on the clinical parameters, it is relevant in development of personalized numerical models, for instance to improve brace design and effects (N. Cobetto et al., 2016; Vergari et al., 2016). The parameters used to validate the method (Table 1) were chosen to be comparable to the previous work by Aubert et al: morphological parameters allow evaluating the shape of the ribs, together with the frontal and sagittal rib orientation, while the clinical parameters were chosen for their clinical interest. For instance, volume and spinal penetration index could be related to respiratory function (Pietton et al., 2017), diameters are of interest in determining subject growth (Dimeglio & Canavese, 2012) while rib hump allows planning and estimating rotation correction by bracing or surgery.

The main limitation of this study is the difficulty of objectively defining "user-friendliness". Users who tested both the present method and its previous implementation reported that painting was easier than choosing single points. However, this was not reflected in shorter reconstruction times. The approach developed in this method did not require counting rib levels, which was a source of error in the previous method; previously, a user would realize that he/she selected the wrong rib level only at the end of the manual identification step, when the initial solution was calculated. In that case, the user had to go back and replace the wrongly identified landmark. In the proposed method, a zoomed-in view on the correct rib insertion was proposed to the operator each time, thus eliminating errors due to rib counting. Another limitation is the relatively small number of included patients (n = 20), which however is consistent with the existing

literature (10 in Grenier et al., 29 in Dworzak et al, 57 in Aubert et al.).

The proposed manual initialization was fast, with an average identification time of less than 2 minutes, which is similar to the previously proposed method (Aubert et al., 2016). However, the current initialization method gave equivalent or better results than the previous one in terms of reproducibility of clinical parameters, and it did not require error-prone counting of rib levels.

Conclusion

The proposed initialization method for rib cage reconstruction has a user-friendly approach, and it provided reliable clinical and morphological parameters. User training and manual labeling are still needed, and the method could be further automatized to reduce human intervention and unavoidable human error. Nevertheless, this work could help facilitate dissemination of quantitative rib cage 3D analysis in clinical routine.

Acknowledgments

The authors are grateful to the ParisTech BiomecAM chair program on subject-specific musculoskeletal modelling for funding (with the support of ParisTech and Yves Cotrel Foundations, Société Générale and Covea). We would also like to thank Ms. Sonia Simoes for her technical help.

References

Aaro, S., & Dahlborn, M. (1981). Estimation of Vertebral Rotation and the Spinal and Rib Cage Deformity in Scoliosis by Computer Tomography. *Spine*, *6*(5). Retrieved from https://journals.lww.com/spinejournal/Fulltext/1981/09000/Estimation_of_Vertebral_Rotation_and_the_Spinal.7.aspx

Aubert, B., Vergari, C., Ilharreborde, B., Courvoisier, A., & Skalli, W. (2016). 3D reconstruction of rib cage geometry from biplanar radiographs using a statistical parametric model approach. *Computer Methods in Biomechanics and Biomedical Engineering: Imaging & Visualization*, *4*(5), 1–15. https://doi.org/10.1080/21681163.2014.913990

Charles, Y. P., Marcoul, A., Schaeffer, M., Canavese, F., & Diméglio, A. (2017). Three-dimensional and volumetric thoracic growth in children with moderate idiopathic scoliosis compared with normal. *Journal of Pediatric Orthopaedics B*, *26*(3), 227–232. https://doi.org/10.1097/BPB.0000000000000393

Cheriet, F., Laporte, C., Kadoury, S., Labelle, H., & Dansereau, J. (2007). A novel system for the 3-D reconstruction of the human spine and rib cage from biplanar X-ray images. *IEEE Transactions on Biomedical Engineering*, *54*(7), 1356–1358. https://doi.org/10.1109/TBME.2006.889205

Cobetto, N., Aubin, C.-E., Clin, J., Le May, S., Desbiens-Blais, F., Labelle, H., & Parent, S. (2014). Braces Optimized With Computer-Assisted Design and Simulations Are Lighter, More Comfortable, and More Efficient Than Plaster-Cast Braces for the Treatment of Adolescent Idiopathic Scoliosis. *Spine Deformity*, *2*(4), 276–284. https://doi.org/http://dx.doi.org/10.1016/j.jspd.2014.03.005

Cobetto, N., Aubin, C. E., Parent, S., Clin, J., Barchi, S., Turgeon, I., & Labelle, H. (2016).

Effectiveness of braces designed using computer-aided design and manufacturing (CAD/CAM) and finite element simulation compared to CAD/CAM only for the conservative treatment of adolescent idiopathic scoliosis: a prospective randomized controlled trial. *European Spine Journal*, *25*(10), 3056–3064. https://doi.org/10.1007/s00586-016-4434-3

Dietrich, T. J., Pfirrmann, C. W. A., Schwab, A., Pankalla, K., & Buck, F. M. (2013). Comparison of radiation dose, workflow, patient comfort and financial break-even of standard digital radiography and a novel biplanar low-dose X-ray system for upright full-length lower limb and whole spine radiography. *Skeletal Radiology*, *42*(7), 959–967. https://doi.org/10.1007/s00256-013-1600-0

Dimeglio, A., & Canavese, F. (2012). The growing spine: how spinal deformities influence normal spine and thoracic cage growth. *European Spine Journal*, *21*(1), 64–70. https://doi.org/10.1007/s00586-011-1983-3

Dubousset, J., Charpak, G., Dorion, I., Skalli, W., Lavaste, F., Deguise, J., … Ferey, S. (2005). [A new 2D and 3D imaging approach to musculoskeletal physiology and pathology with low-dose radiation and the standing position: the EOS system]. *Bull Acad Natl Med*, *189*(2), 287–300. Retrieved from http://www.ncbi.nlm.nih.gov/pubmed/16114859

Dubousset, J., Ilharreborde, B., & Le Huec, J.-C. (2014). Use of EOS imaging for the assessment of scoliosis deformities: application to postoperative 3D quantitative analysis of the trunk. *European Spine Journal*, *23*(4), 397–405. https://doi.org/10.1007/s00586-014-3334-7

Dworzak, J., Lamecker, H., Berg, J., Klinder, T., Lorenz, C., Kainmüller, D., … Zachow, S. (2010). 3D reconstruction of the human rib cage from 2D projection images using a statistical shape model. *International Journal of Computer Assisted Radiology and Surgery*, *5*(2), 111–124. https://doi.org/10.1007/s11548-009-0390-2

Ferrero, E., Lafage, R., Vira, S., Rohan, P.-Y., Oren, J., Delsole, E., … Skalli, W. (2017). Three-dimensional reconstruction using stereoradiography for evaluating adult spinal deformity: a reproducibility study. *European Spine Journal*, *26*(8), 2112–2120. https://doi.org/10.1007/s00586-016-4833-5

Ghostine, B., Sauret, C., Assi, A., Bakouny, Z., Khalil, N., Skalli, W., & Ghanem, I. (2017). Influence of patient axial malpositioning on the trueness and precision of pelvic parameters obtained from 3D reconstructions based on biplanar radiographs. *European Radiology*, *27*(3), 1295–1302. https://doi.org/10.1007/s00330-016-4452-x

Glaser, D. A., Doan, J., & Newton, P. O. (2012). Comparison of 3-Dimensional Spinal Reconstruction Accuracy: Biplanar Radiographs With EOS Versus Computed Tomography. *Spine*, *37*(16). Retrieved from https://journals.lww.com/spinejournal/Fulltext/2012/07150/Comparison_of_3_Dimensional_Spinal_Reconstruction.8.aspx

Gréalou, L., Aubin, C. E., & Labelle, H. (2002). Rib cage surgery for the treatment of scoliosis: a biomechanical study of correction mechanisms. *Journal of Orthopaedic Research : Official Publication of the Orthopaedic Research Society*, *20*(5), 1121–1128. https://doi.org/10.1016/S0736-0266(02)00010-4

Grenier, S., Parent, S., & Cheriet, F. (2013). Personalized 3D reconstruction of the rib cage for clinical assessment of trunk deformities. *Medical Engineering & Physics*, *35*(11), 1651–1658. https://doi.org/10.1016/j.medengphy.2013.06.002

Hocquelet, A., Cornelis, F., Jirot, A., Castaings, L., de Sèze, M., & Hauger, O. (2016). Patient-specific 3D models created by 3D imaging system or bi-planar imaging coupled with Moiré-

-Fringe projections: a comparative study of accuracy and reliability on spinal curvatures and vertebral rotation data. *European Spine Journal*, *25*(10), 3154–3161. https://doi.org/10.1007/s00586-016-4659-1

Humbert, L., De Guise, J. A., Aubert, B., Godbout, B., & Skalli, W. (2009). 3D reconstruction of the spine from biplanar X-rays using parametric models based on transversal and longitudinal inferences. *Med Eng Phys*, *31*(6), 681–687. https://doi.org/10.1016/j.medengphy.2009.01.003

Ilharreborde, B., Steffen, J. S., Nectoux, E., Vital, J. M., Mazda, K., Skalli, W., & Obeid, I. (2011). Angle measurement reproducibility using EOS three-dimensional reconstructions in adolescent idiopathic scoliosis treated by posterior instrumentation. *Spine (Phila Pa 1976)*, *36*(20), E1306-13. Retrieved from http://europepmc.org/abstract/MED/21697768

Jolivet, E., Sandoz, B., Laporte, S., Mitton, D., & Skalli, W. (2010). Fast 3D reconstruction of the rib cage from biplanar radiographs. *Medical and Biological Engineering and Computing*, *48*(8), 821–828. https://doi.org/10.1007/s11517-010-0610-5

Macovski, A. (1983). *Medical Imaging Systems*. Englewood Cliffs, NJ: Prentice-Hall.

Mitton, D., Zhao, K., Bertrand, S., Zhao, C., Laporte, S., Yang, C., … Skalli, W. (2008). 3D reconstruction of the ribs from lateral and frontal X-rays in comparison to 3D CT-scan reconstruction. *Journal of Biomechanics*, *41*(3), 706–710. https://doi.org/10.1016/j.jbiomech.2007.09.034

Nankali, S., Torshabi, A. E., & Miandoab, P. S. (2017). A Feasibility Study on Ribs as Anatomical Landmarks for Motion Tracking of Lung and Liver Tumors at External Beam Radiotherapy. *Technology in Cancer Research & Treatment*, *16*(1), 99–111. https://doi.org/10.1177/1533034615595737

Pietton, R., Bouloussa, H., Vergari, C., Skalli, W., & Vialle, R. (2017). Rib Cage Measurement Reproducibility Using Biplanar Stereoradiographic 3D Reconstructions in Adolescent Idiopathic Scoliosis. *Journal of Pediatric Orthopedics*. https://doi.org/10.1097/bpo.0000000000001095

Rousseau, M.-A., Brusson, A., & Lazennec, J.-Y. (2014). Assessment of the axial rotation of the pelvis with the EOS® imaging system: intra- and inter-observer reproducibility and accuracy study. *European Journal of Orthopaedic Surgery & Traumatology*, *24*(6), 891–895. https://doi.org/10.1007/s00590-013-1281-3

Sabourin, M., Jolivet, E., Miladi, L., Wicart, P., Rampal, V., & Skalli, W. (2010). Three-dimensional stereoradiographic modeling of rib cage before and after spinal growing rod procedures in early-onset scoliosis. *Clinical Biomechanics (Bristol, Avon)*, *25*(4), 284–291. https://doi.org/10.1016/j.clinbiomech.2010.01.007

Seoud, L., Cheriet, F., Labelle, H., & Dansereau, J. (2011). A novel method for the 3-D reconstruction of scoliotic ribs from frontal and lateral radiographs. *IEEE Transactions on Biomedical Engineering*, *58*(5), 1135–1146. https://doi.org/10.1109/TBME.2009.2032530

Serrurier, A., Quijano, S., Nizard, R., & Skalli, W. (2012). Robust femur condyle disambiguation on biplanar X-rays. *Medical Engineering and Physics*, *34*, 1433–1440. https://doi.org/10.1016/j.medengphy.2012.01.008

Thulbourne, T., & Gillespie, R. (1976). The rib hump in idiopathic scoliosis. Measurement, analysis and response to treatment. *Bone & Joint Journal*, *58–B*(1), 64–71. Retrieved from http://bjj.boneandjoint.org.uk/content/58-B/1/64

Tones, M., Moss, N., & Polly, D. W. J. (2006). A Review of Quality of Life and Psychosocial

Issues in Scoliosis. *Spine*, *31*(26). Retrieved from https://journals.lww.com/spinejournal/Fulltext/2006/12150/A_Review_of_Quality_of_Life_and_Psychosocial.9.aspx

Vergari, C., Courtois, I., Ebermeyer, E., Bouloussa, H., Vialle, R., & Skalli, W. (2016). Experimental validation of a patient-specific model of orthotic action in adolescent idiopathic scoliosis. *European Spine Journal*, *25*(10), 3049–3055. https://doi.org/10.1007/s00586-016-4511-7

Vergari, C., Ribes, G., Aubert, B., Adam, C., Miladi, L., Ilharreborde, B., … Skalli, W. (2015). Evaluation of a patient-specific finite element model to simulate conservative treatment in adolescent idiopathic scoliosis. *Spine Deformity*, *3*(1), 4–11. https://doi.org/http://dx.doi.org/10.1016/j.jspd.2014.06.014

Weinstein, S. L., Dolan, L. A., Cheng, J. C., Danielsson, A., & Morcuende, J. A. (2008). Adolescent idiopathic scoliosis. *Lancet*, *371*(9623), 1527–1537. https://doi.org/10.1016/S0140-6736(08)60658-3

Yaszay, B., Bastrom, T. P., Bartley, C. E., Parent, S., & Newton, P. O. (2017). The effects of the three-dimensional deformity of adolescent idiopathic scoliosis on pulmonary function. *European Spine Journal*, *26*(6), 1658–1664. https://doi.org/10.1007/s00586-016-4694-y